[American Journal of Science, Vol. 316, January, 2016, P. 64–83, DOI 10.2475/01.2016.02]

A CENOZOIC SEAWATER REDOX RECORD DERIVED FROM $^{238}U/^{235}U$ IN FERROMANGANESE CRUSTS

XIANGLI WANG*,§,†, NOAH J. PLANAVSKY*, CHRISTOPHER T. REINHARD**, JAMES R. HEIN***, and THOMAS M. JOHNSON§

ABSTRACT. Oceanic oxygen levels are projected to drop in certain areas due to warming climate, but the net effect to the overall ocean redox state is difficult to predict. Here we measured the "stable" uranium isotope composition ($^{238}U/^{235}U$) in globally representative hydrogenous ferromanganese crusts in order to reconstruct the redox evolution of the global ocean throughout the Cenozoic. Samples averaging ~3 Myr intervals have analytically indistinguishable $^{238}U/^{235}U$ throughout the Cenozoic. Combined with a U isotope mass balance model, we suggest that the overall ocean redox state has remained remarkably stable on million year time scales throughout the Cenozoic, despite large surface temperature fluctuations during this time. This suggests that stabilizing feedbacks (for example, nutrient limitation in low oxygen zones) may have prevented dramatic large-scale shifts in oxygen levels in the ocean. However, the Fe-Mn crust record will be unlikely to reflect rapid perturbations in ocean redox state. To investigate these events, sediment archives with faster accumulation rates and redox proxies with faster response time must be explored.

Keywords: Uranium isotopes, redox proxies, Cenozoic marine redox

INTRODUCTION

Models predict that warmer surface temperatures will reduce O_2 solubility and potentially increase thermal stratification in Earth's oceans (Sarmiento and others, 1998; Shaffer and others, 2009), potentially leading to ocean "deoxygenation" on a broad scale (for examples, Keeling and others, 2010). However, a general lack of well-established long-term and globally representative ocean redox records hinders understanding of potential feedbacks that regulate the spatial extent of low oxygen and/or anoxic marine conditions. Here we apply a uranium isotope approach ($^{238}U/^{235}U$, expressed as $\delta^{238}U$ relative to the standard CRM112a) to hydrogenous ferromanganese (Fe-Mn) crusts in order to reconstruct ocean redox state throughout the Cenozoic [65 million years (Myr) ago to the present], a period during which tectonism, weathering, and surface temperatures fluctuated significantly (Hansen and others, 2008). A similar approach was employed by Goto and others (2014), but this record was derived from a single ocean basin and only extends back to 45 Myr ago. In addition, Goto and others (2014) could not rule out diffusional overprinting of the temporal isotope record. In this work we expand the record both spatially (to three major ocean basins) and temporally (to ~77 Myr ago) while ruling out an overriding control by diffusional overprinting.

Uranium isotopes have been recently proposed as an oceanographic redox proxy that can be used to track anoxic ocean conditions (Andersen and others, 2014 and references therein). Uranium has two valence states in surface environments: the soluble U(VI) and insoluble U(IV) (Langmuir, 1978). Under reducing conditions U(VI) is reductively removed from seawater. This process results in ^{238}U becoming enriched in the reduced phase, causing the remaining dissolved U(VI) in seawater to

* Yale University, Department of Geology and Geophysics, New Haven, Connecticut, 06520-8109 USA
** Georgia Institute of Technology, School of Earth and Atmospheric Sciences, Atlanta, Georgia, 30332 USA
*** US Geological Survey, PCMSC, Santa Cruz, California, 95060 USA
§ University of Illinois, Department of Geology, Urbana-Champaign, Illinois, 61820 USA
† Corresponding author: xiangli.wang@yale.edu

be fractionated to lower $^{238}U/^{235}U$ values. This trend of fractionation—opposite to traditional mass-dependent fractionation—has been well constrained by both empirical observation (Stylo and others, 2015 and references there in) and theoretical prediction based on "nuclear volume effect" (for example, Schauble, 2007). Therefore, at steady state—a condition likely applicable to the modern ocean (Andersen and others, 2016)—the $^{238}U/^{235}U$ of seawater is expected to shift to lower values when ocean basins characterized by reducing conditions expand.

Strictly speaking, $^{238}U/^{235}U$ only tracks benthic redox conditions. This is because U(VI) reduction tends to occur below the sediment-water interface rather than within the water column (Anderson and others, 1989; Barnes and Cochran, 1990). However, it is expected that changes in the areal extent of benthic anoxia are difficult to accomplish without significant changes to the volume of Oxygen Minimum Zones (OMZs) in the water column. The reason is that most of anoxic seafloor in the modern open ocean—with the exception of restricted basins such as the Black Sea—is a result of OMZs impinging on the seafloor below coastal upwelling zones (Helly and Levin, 2004; Paulmier and Ruiz-Pino, 2009; Stramma and others, 2010). Because the residence time of U is much longer (~400 kyr, Ku and others, 1977) than timescales of ocean mixing (~1 kyr, Broecker and Peng, 1982), it is expected that the U concentration and isotopic composition will be essentially homogeneous in the ocean. Therefore, the U isotope system can potentially track ocean anoxia on a global scale.

Seafloor Fe-Mn crusts provide a powerful archive for seawater chemistry because they precipitate directly from seawater and preferentially incorporate a wide range of trace elements (see Frank and others, 1999; Koschinsky and Hein, 2003; Siebert and others, 2003; Rehkämper and others, 2004; Hein and Koschinsky, 2014). Goto and others (2014) measured the surface layers of 19 Fe-Mn crusts dredged from the Pacific Ocean and obtained similar $\delta^{238}U$ values of -0.65±0.05‰ (2SD, n=19). This value is offset from the modern seawater $\delta^{238}U$ (-0.41‰) by -0.24 permil, which agrees well with experimental determination of U isotopic fractionation during adsorption of U(VI) to manganese oxides (Brennecka and others, 2011b). Therefore, both field and experimental studies suggest that Fe-Mn crusts can record contemporaneous seawater $\delta^{238}U$, taking the fractionation attendant to adsorption to Mn-oxide surfaces into account.

SAMPLES AND METHODS

The Fe-Mn crusts examined in this study include: ANTP109D-E and DODO232D-B from the Indian Ocean, D11-1 and CD29-2 from the Pacific Ocean, and ALV539 from the Atlantic Ocean (table 1, fig. 1). Crusts (4–15 cm thick) were embedded in resin and cut perpendicular to the growth layers. The exposed depth profile was sampled by micro drilling (~4 mm^2 drilling area) to obtain ~30 to 120 mg of material at temporal resolutions ranging from 1.2 to 12.1 Myr (table 2). The resolution is limited by the thickness—and thus accumulation rate—of the crusts. Drilled powders were dissolved in 4 mL 6N HCl for ~10 hours at room temperature. The amount of detrital grains undissolved by the 6 N HCl accounted for very small portions (<1%) of the total sample materials.

Analytical details are described in the Appendix. Briefly, U was extracted from the sample digests using the UTEVA ion exchange and ^{233}U-^{236}U double-spike method (Chen and Wasserburg, 1981; Horwitz and others, 1993; Stirling and others, 2005; Rademacher and others, 2006; Weyer and others, 2008). Uranium isotopic compositions were measured on a Nu Plasma multicollector ICP-MS, with instrument parameters described in Wang and others (2015). Procedural blanks were 10 to 40 pg, which were negligible (<0.01%) compared to 300 ng sample U. External uncertainties for $\delta^{238}U$, U concentration, and $^{234}U/^{238}U$ activity ratio (see result section) measurements were ±0.07‰, ±0.1 ìg/g, and 3.7 permil at 95 percent confidence level, respectively,

TABLE 1

Basic information for the Fe-Mn crusts examined in this study

	Section (mm), top=0	Growth Rate (mm/Myr)	[U] (μg/g)	Latitude	Longitude	Ocean	Water depth (m)	Refs.
D11-1	0–60	1.7	13.6	11°38.9' N	161°40.5' E	W. Pacific	1870-1690	(4)
	60–132	3.8	11.2					
	132–168.5	1.6	9.8					
CD29-2	All	2.1	9.4	16° 42' N	168° 14' W	Pacific	2390-1970	(1)
ALV539	0–29.5	2.4	5.5	35°36.4' N	58°47.1' W	N. Atlantic	2665	(2)
	29.5–90.5	3.3	8.0					
ANTP109D-E	0–12	2.4	8.6	27° 58.4' S	60° 47.8' E	Indian Oc.	5689-5178	(3)
	12–36	3.3	6.9					
DODO232D-B	All	4.3	6.5	5° 23' S	97° 29' E	Indian Oc.	4119	(5)

General information and age models used to calculate growth rates can be found in refs. (1)Klemm and others, 2005; (2) Klemm and others, 2008; (3) Nielsen and others, 2011; (4) Nielsen and others, 2009; (5) Rehkämper and others, 2002.

Growth rates are derived from Os chemostratigraphy except for DODO232-D-B, whose age is constrained by cosmogenic ^{10}Be and Co flux method (see text in "Age Models" section). U concentration data of individual samples can be found in table 2.

calculated as the root mean square difference (Hyslop and White, 2009) of six duplicate sample preparations and analyses.

AGE MODELS

Age models for the examined Fe-Mn crusts are derived from ^{187}Os/^{188}Os, T1 chemostratigraphy, and cosmogenic ^{10}Be methods. Since the development of a

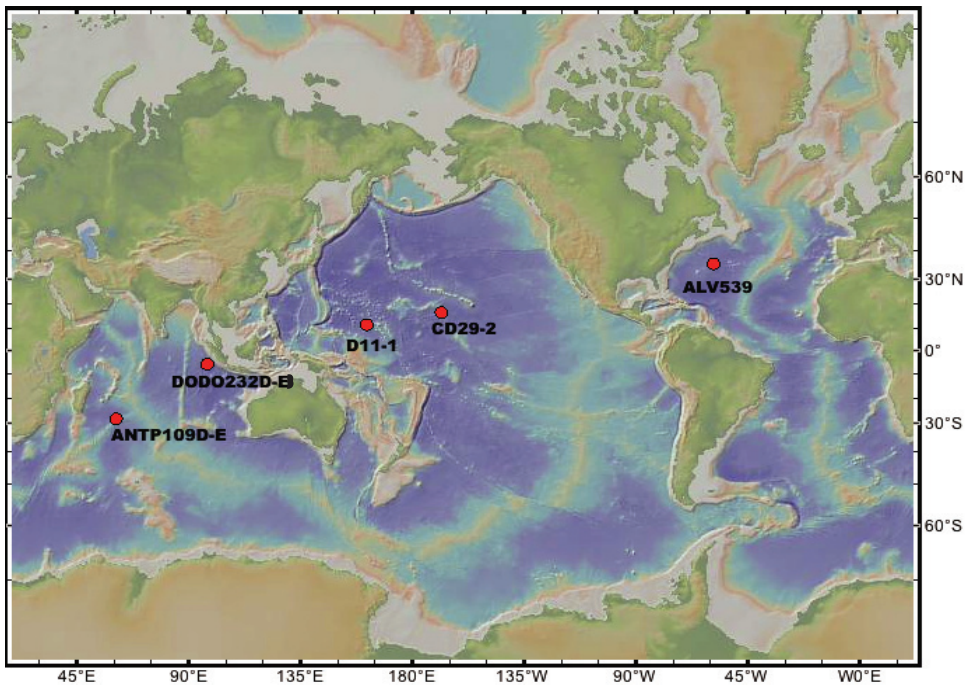

Fig. 1. Map showing the locations of the Fe-Mn crusts examined here.

reliable seawater osmium isotope record (see Klemm and others, 2005 for a review), Os chemostratigraphic correlation has been used to date Fe-Mn crusts. Prior to this, age models for Fe-Mn crusts were mainly constructed using cosmogenic ^{10}Be for the past 10 Myr and extrapolated to older ages assuming uniform accumulation rates (O'Nions and others, 1998; Frank and others, 1999; Rehkämper and others, 2004). This extrapolation was supplemented by a Co flux dating method (Puteanus and Halbach, 1988; Frank and others, 1999). In many cases, large discrepancies were recognized between Be/Co and Os age models, especially for older layers (Klemm and others, 2005; Burton, 2006; Klemm and others, 2008; Nielsen and others, 2009; Nielsen and others, 2011). For instance, the Os isotope technique enabled several growth hiatuses to be identified (Klemm and others, 2005; Nielsen and others, 2009). Three of our five examined crusts have published Os-based ages (CD29-2, Klemm and others, 2005; ALV539, Klemm and others, 2008; ANTP109D-E, Nielsen and others, 2011) and therefore the Os age models were used. Ages for crust D11-1 is based on T1 isotope record (Nielsen and others, 2009). Ages for crust CD29-2 is based on Be/Co methods (Rehkämper and others, 2004). The average growth rates based on these age models are summarized in table 1.

RESULTS

The measured $\delta^{238}U$ values in all five Fe-Mn crusts fall within a close range, with an average of -0.61±0.09‰ (2SD, n=52, fig. 2 and table 2). The average $\delta^{238}U$ value is ~0.2 permil lower than the modern seawater value of -0.4 permil (Weyer and others, 2008), consistent with previous measurements of the surface layers of Fe-Mn crusts (Weyer and others, 2008; Goto and others, 2014) and previous experimental work on adsorption of U(VI) onto Mn oxides (Brennecka and others, 2011b). A systematic trend in crust DODO232D-B appears to exist but is constant within error. This apparent trend is not seen in any of the other studied crusts, so we will not address it further.

It is crucial to consider open-system behavior of U in Fe-Mn crusts, and this can be assessed through U-series disequilibrium (for example, Henderson and Burton, 1999). Briefly (see Bourdon and others, 2003 for details), in the U-Th decay chain, ^{238}U (half-life=4.46 Gyr, Jaffey and others, 1971) decays through two very short-lived intermediate nuclides (^{234}Th and ^{234}Pa) to form ^{234}U (half-life=245 kyr, Cheng and others, 2000), which further decays to form ^{230}Th. Regardless of the relative amount of ^{238}U, ^{234}U and ^{230}Th that the decay chain starts with, as long as it is not disturbed, it will eventually reach equilibrium (referred to as *secular equilibrium*). At secular equilibrium, the number of decays per unit time—termed *activity*—for ^{238}U equals that for ^{234}U, thus their activity ratio—expressed as ($^{234}U/^{238}U$)—equals 1. The time needed to reach ^{234}U-^{238}U secular equilibrium is ~1 Myr, determined by the half-life of the relatively shorter-lived ^{234}U. In other words, regardless of the initial ($^{234}U/^{238}U$) value of a sample, so long as it behaves as a closed system for more than ~1 Myr, its ($^{234}U/^{238}U$) value should be ~1. Modern seawater has a ($^{234}U/^{238}U$) value of ~1.14, due to alpha-recoil ejection of ^{234}Th—and thus ^{234}Pa and ^{234}U— into weathering fluids and ultimately seawater (for example, Henderson, 2002; DePaolo and others, 2006). If a sample has ($^{234}U/^{238}U$) values significantly above the secular equilibrium value of 1, it means there has been open system behavior in the last ~1 Myr, most likely due to diffusion of modern seawater into the interior of Fe-Mn crust. The ($^{234}U/^{238}U$) values in most Fe-Mn crust samples explored here are distinct from the modern seawater value and are close to the secular equilibrium value of 1 (fig. 3). Some of the data points are even below the secular equilibrium value—presumably due to the effects of local alpha-recoil. However, Fe-Mn crusts formed in the last 3 Myr yield ($^{234}U/^{238}U$) values higher than 1, indicating influence by modern seawater. However,

TABLE 2

Results for U isotopic compositions and concentrations

Name	Depth (mmbs[a])	Age[b] (Myr)	$\delta^{238}U$ (‰)	Error[c] (‰)	$(^{234}U/^{238}U)$[d]	U (μg/g)[e]
D11-1	3	1.7	-0.65	0.07	1.029	13.4
	11.5	5.4	-0.66	0.07	0.952	12.6
	11.5-dup		-0.66	0.07	0.925	12.6
	34.5	17.6	-0.59	0.07	0.951	14.9
	64.5	34.0	-0.59	0.07	0.996	12.3
	90.0	43.0	-0.63	0.07	0.971	10.6
	90.0-dup		-0.67	0.10	0.940	10.5
	120.5	51.0	-0.54	0.07	1.029	10.7
	143.5	59.0	-0.54	0.07	0.952	12.3
	169.0	76.8	-0.62	0.07	0.968	7.3
ALV539	6.5	2.7	-0.58	0.07	1.017	3.6
	15.5	6.5	-0.62	0.07	0.999	5.5
	25.5	10.8	-0.59	0.07	1.000	7.4
	34.5	14.1	-0.62	0.07	1.006	6.9
	45.5	17.2	-0.63	0.07	1.017	6.9
	55.5	20.2	-0.62	0.07	1.015	7.9
	65.5	23.2	-0.54	0.07	1.016	7.9
	74.5	26.0	-0.61	0.07	1.024	8.6
	84.5	29.0	-0.59	0.07	1.043	9.8
ANTP109D-E	2.5	1.0	-0.65	0.07	0.969	8.8
	2.5-dup		-0.63	0.07	0.956	8.9
	6.5	2.9	-0.61	0.07	0.948	9.0
	10.5	4.8	-0.57	0.07	0.973	7.8
	14.5	5.3	-0.59	0.07	0.964	8.2
	19.5	5.7	-0.61	0.07	0.954	6.9
	24.5	5.9	-0.60	0.07	0.969	5.9
	29.5	6.1	-0.66	0.07	0.991	8.1
	33.5	6.4	-0.60	0.07	1.033	6.8
	38.5	6.5	-0.61	0.09	0.969	5.4
CD29-2	3.5	1.7	-0.55	0.10	0.911	11.4
	3.5-dup		-0.63	0.07	0.905	11.4
	13.5	6.4	-0.60	0.07	0.926	11.0
	25.5	12.1	-0.59	0.07	0.965	9.4
	35	31.7	-0.61	0.08	0.996	9.2
	44.5	39.2	-0.60	0.07	0.947	8.6
	55.5	48.4	-0.61	0.07	0.945	9.0
	65.5	53.2	-0.58	0.07	0.921	6.3
	65.5-dup		-0.57	0.07	0.936	6.3
	74.5	57.5	-0.66	0.09	0.947	8.9
	84.5	62.2	-0.64	0.07	1.029	9.8
	92.5	66.0	-0.54	0.07	0.911	10.8
	103	70.8	-0.58	0.07	0.905	8.9

TABLE 2
(continued)

Name	Depth (mmbs[a])	Age[b] (Myr)	$\delta^{238}U$ (‰)	Error[c] (‰)	$(^{234}U/^{238}U)$[d]	U (μg/g)[e]
DODO232D-B	2.5	*0.6*	-0.60	0.07	0.951	8.0
	7.5	*1.7*	-0.52	0.11	0.939	7.0
	7.5-dup		-0.59	0.07	0.953	7.0
	14.5	*3.4*	-0.60	0.07	0.959	7.5
	21.5	*5.0*	-0.66	0.07	0.973	7.0
	28.5	*6.6*	-0.67	0.07	0.975	6.6
	36.5	*8.5*	-0.71	0.07	0.986	6.1
	45	*10.5*	-0.71	0.07	0.996	6.2
	53.5	*12.4*	-0.71	0.07	1.029	5.4
	61.5	*14.3*	-0.67	0.07	1.084	5.8
	68.5	*15.9*	-0.57	0.07	0.951	5.2

[a]Millimeter below crust surface; [b]Os-based ages except for crust DODO232D-B, which is based on cosmogenic ^{10}Be ages extended by Co method (see text); [c]Errors (95% confidence) are either the internal 2 standard errors based on counting statistics or external uncertainty calculated as the root mean square difference (Hyslop and White, 2009) of the six duplicate preparations and analyses, whichever is greater; [d]external precision (2 root mean square difference) on $(^{234}U/^{238}U)$ measurement is 0.37%. "Lat", "Lon.", and "Dep." are short for latitude, longitude, and depth. [e]Concentrations were derived from isotope dilution method.

such diffusional overprinting seems to have affected only the surface 1 to 2 mm layer of all crusts examined here, except for ALV539 which has elevated $(^{234}U/^{238}U)$ values on the surface and deeper parts, but secular equilibrium values in the middle. The latter pattern is most likely due to bottom-up diffusion of modern seawater through the underlying substrate (Goto and others, 2014).

U concentrations (fig. 4) reveal the following observations: (1) they vary among crusts from different oceans; (2) they vary temporally within the same crust; (3) the time series do not correlate among crusts. For example, in the past 20 Myr, crusts ANTP109D-E, DODO232D-B and CD29-2 show decreasing trends, while ALV539 and D11-1 show the opposite. These observations suggest that the U concentrations in these Fe-Mn crusts are controlled primarily by growth processes, rather than by temporal changes in seawater U concentrations. In general, lower growth rates seem to be associated with higher U concentrations (fig. 4). There is no correlation among $\delta^{238}U$, $(^{234}U/^{238}U)$, and U concentration (not shown).

DISCUSSION

Phosphatization

During periods of global climate change throughout the Paleogene, previously formed Fe-Mn crusts were impregnated with carbonate fluorapatite (Hein and others, 1993), potentially altering original U isotope signatures. Phosphatization typically affects crusts formed at water depths shallower than ~2500 m. Therefore, among the five crusts studied, only the older layers of crusts D11-1 and CD29-2 were phosphatized (Ling and others, 1997). Phosphatization has been known to affect the redistribution of some elements in Mn-Fe crusts, such as Pb and Sr (Koschinsky and Halbach, 1995; Hein and Koschinsky, 2014), but does not seem to change the isotopic ratio of the elements studied thus far (Frank and others, 1999; Rehkämper and others, 2004). Most importantly, the absence of an inflection in the $\delta^{238}U$ curve at the phosphatization boundary in D11-1 and CD29-2 indicates that the $\delta^{238}U$ signature was not strongly affected by phosphatization.

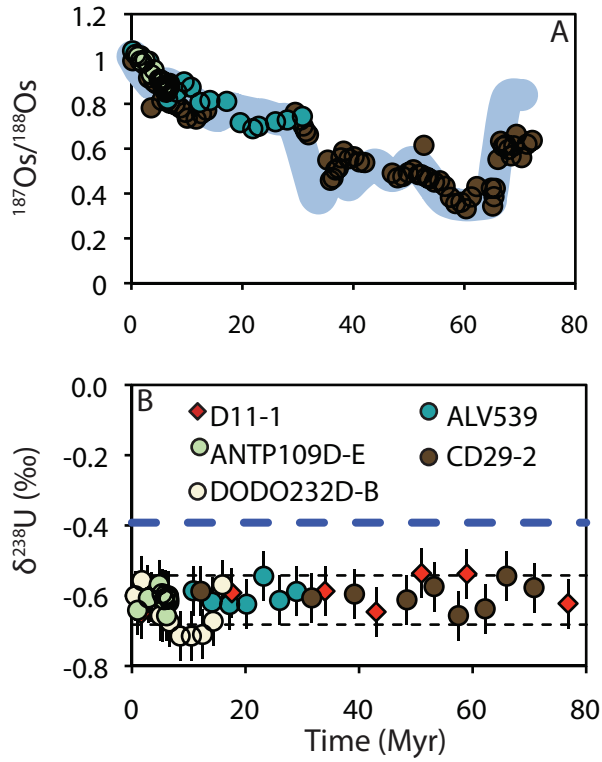

Fig. 2. Results for $\delta^{238}U$ in Fe-Mn crusts (B) and previously published Os isotope data (A) for the seawater (shaded band) and the same Fe-Mn crusts. Modern seawater $\delta^{238}U$ value is indicated by the thick dashed line (Tissot and Dauphas, 2015 and references therein). The two black thin dashed lines represent the 2σ (±0.07‰) surrounding the mean value (-0.61‰). The fact that Os isotope data in the Fe-Mn crusts align well with the seawater Os data suggests that the Os isotopic compositions in Fe-Mn crusts are not altered by the modern water. Given that Os diffuses ~30 times faster than U in Fe-Mn crust (Henderson and Burton, 1999), this provides strong evidence that the invariable U isotope trend is a primary signature rather than diffusional artifact. Os data sources: CD29-2, Klemm and others, 2005; ALV539, Klemm and others, 2008; ANTP109D-E, Nielsen and others, 2011; seawater, reviewed in Klemm and others, 2005.

Diffusional Overprinting

In all five of the Fe-Mn crusts examined in this study, the layers deposited within the last ~3 Myr have ($^{234}U/^{238}U$) values slightly above the theoretical decay trajectory (fig. 3). Since the ages of the younger intervals are well constrained by the cosmogenic ^{10}Be and $^{187}Os/^{188}Os$ methods, such mismatch is not likely explainable by errors on age constraints and is more likely due to addition of ^{234}U from modern seawater, which has a ($^{234}U/^{238}U$) of ~1.14 (Ku and others, 1977; Henderson and Burton, 1999). As seawater diffuses inward along the grain boundary, ^{234}U is concurrently consumed by decay. If diffusion is faster than decay, then ^{234}U would accumulate and we would expect to observe ($^{234}U/^{238}U$) above the theoretical decay curve. We think this is true for the younger layers (<3 Myr) of Fe-Mn crusts (fig. 3). The fact that elevated ($^{234}U/^{238}U$) was observed in young layers but not older layers can be explained by two possible scenarios: (1) The penetration length scale of diffusive influence is on the order of ~1 to 2 mm and thus only the young layers are affected; (2) diffusion advances further into the interior of the crust, but the timescale of diffusion beyond ~1 to 2 mm into the Fe-Mn crust is long enough for secular equilibrium to be achieved, and

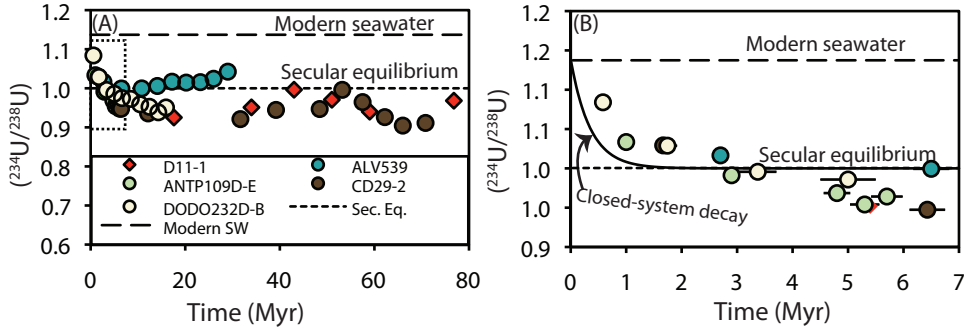

Fig. 3. $^{234}U/^{238}U$ activity ratio, represented as ($^{234}U/^{238}U$), as a monitor of diffusional overprinting by modern seawater. The upper and lower horizontal dashed lines in (A and B) represent modern seawater value and secular equilibrium value of 1.14 and 1, respectively (Ku and others, 1977). (B) shows magnified details of the rectangular area in (A), with the black curve showing the theoretical ($^{234}U/^{238}U$) evolution in a closed system (calculated using half-lives from Cheng and others, 2013). Error bars for ($^{234}U/^{238}U$) are smaller than symbols. Larger age error bars for DODO232D-B are due to lack of Os chemostratigraphy.

therefore ($^{234}U/^{238}U$) appears as if there was no diffusion despite overprinting of $\delta^{238}U$ values by recent seawater throughout the crust.

The second model implies that the absence of elevated ($^{234}U/^{238}U$) in older Fe-Mn crust layers cannot be treated as firm evidence that $\delta^{238}U$ values have not been overprinted. However, Fe-Mn crusts are taken to faithfully record the seawater $^{187}Os/^{188}Os$ trend derived from independent archives (fig. 2). For the U concentrations observed in our Fe-Mn crusts, the effective diffusivity of U in the crust should be on the order of ~30 times less rapid than that of Os (for example, Henderson and Burton, 1999). As a result, there is no readily available mechanistic explanation for overprinting the $\delta^{238}U$ record throughout the crust by recent seawater while simultaneously leaving the $^{187}Os/^{188}Os$ system unperturbed. Furthermore, the large temporal variations in U content (fig. 4) in all of the crusts examined here also argue against diffusional overprinting, which would tend to systematically smooth out the temporal

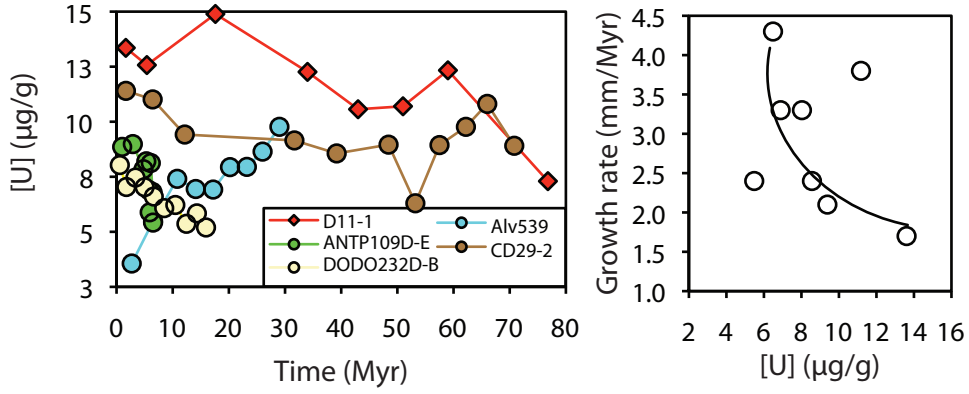

Fig. 4. U concentration for the examined Fe-Mn crusts. No correlation was found among individual crusts, suggesting crust U concentration is not controlled by seawater U concentration but by formation mechanisms. Lower growth rates based on cosmogenic ^{10}Be and Co fluxing methods seem to correlate to higher U concentration, with only one data point falling off the trend. No correlations were found among U concentration, $\delta^{238}U$ and ($^{234}U/^{238}U$) data (plots not shown).

trends. Therefore, the most plausible explanation for the stability of the $\delta^{238}U$ record is that on timescales of ~3 Myr, the Fe-Mn crusts examined here provide a robust archive for seawater $\delta^{238}U$ composition that has remained essentially unchanged throughout the Cenozoic.

Uranium Isotope Mass Balance Modeling

In order to quantitatively relate our seawater U isotope record to the spatial extent of benthic ocean anoxia, we construct a simple isotope mass balance model designed to explore the sensitivity of the U isotope system to shifts in ocean redox state. Our modeling approach differs in design and purpose from similar recent treatments. Goto and others (2014) aimed to investigate the effect of metallic sediment production on seawater $\delta^{238}U$, whereas Tissot and Dauphas (2015) focused on testing the robustness of various ocean U budgets. In contrast, our goal is to explicitly examine the sensitivity of seawater $\delta^{238}U$ to changing relative proportions of oxic, suboxic, and anoxic/euxinic seafloor. In essence, our principle aim is to quantify how our current analytical uncertainty on $\delta^{238}U$ measurement ($\pm 0.07‰$) translates into changing ocean redox conditions.

Following Goto and others (2014) and references therein, transient global seawater [U] and $\delta^{238}U$ can be written as:

$$dM_{SW}/dt = F_r - \Sigma F_i \quad (1)$$

$$d(M_{SW}\delta_{SW})/dt = F_r\delta_r - \Sigma F_i(\delta_{SW} + \Delta_i) \quad (2)$$

where M_{SW} refers to the mass of U in seawater; F_r represents the river input flux and F_i represents anoxic, suboxic, and oxic sink fluxes (mol yr^{-1}); δ_{SW} and δr refer to the $\delta^{238}U$ values of seawater and the river input; Δ_i refers to isotopic fractionation factors for anoxic, suboxic, and oxic sinks. At steady state (Andersen and others, 2016), the left side of equation (1) and (2) equals 0, yielding:

$$F_r = \Sigma F_i \quad (3)$$

$$\delta_{SW} = \delta_r - \Sigma f_i\Delta_i \quad (4)$$

where f_i is the fraction of individual sink fluxes out of the total input flux: $f_i = F_i/F_r$. If we assume that removal mechanisms are first order with respect to seawater U concentration (Hastings and others, 1996; Partin and others, 2013; Reinhard and others, 2013), we have

$$F_i = k_i A_i[U] \quad (5)$$

where A_i represents the seafloor areas covered by various sinks; [U] denotes seawater U concentration, and k_i terms are effective burial rate constants solved for by inverting modern areas and burial fluxes (see table 3).

Parameters used in our modeling exercises are listed in table 3 and schematically shown in figure 5. Following previous studies (Montoya-Pino and others, 2010; Brennecka and others, 2011a; Goto and others, 2014), the riverine input flux (F_r) is considered to be the dominant source of U to the ocean—aeolian and subsea groundwater discharges are ignored because of their relatively small contributions. Burial sinks for U are divided into anoxic/sulfidic (F_{anox}), suboxic (F_{subox}) and oxic (F_{ox}) sinks (Barnes and Cochran, 1990; Dunk and others, 2002). Note that anoxic/sulfidic, suboxic and oxic are referring to the porewater redox, not the overlying water column. This classification scheme was first proposed by Berner (1981) and used by many subsequent studies (for example, Murray and others, 2007). Specifically, anoxic is defined as $[O_2] = [H_2S] \approx 0$ μmol/L, sulfidic as $[O_2] = 0$ μmol/L and $[H_2S] \geq 11$

TABLE 3

Parameters used in the mass balance model

Parameter	Description	Value	Unit	Refs.
F_r	Riverine U fluxes to oceans	4.2×10^{7}	mol/yr	(2), (3), (10), (11)
F_{ox}	Removal flux to oxic sinks	2.23×10^{7}	mol/yr	(2), (3), (10), (11)
F_{subox}	Removal flux to suboxic sinks	1.53×10^{7}	mol/yr	(2), (3), (10), (11)
F_{anox}	Removal flux to anoxic sinks	4.45×10^{6}	mol/yr	(2), (3), (10), (11)
k_{ox}	Effective burial rate constant for oxic sink	0.048	1/(dm*yr)	*
k_{subox}	Effective burial rate constant for suboxic sink	0.469	1/(dm*yr)	*
k_{anox}	Effective burial rate constant for anoxic sink	2.534	1/(dm*yr)	*
δ_r	$\delta^{238}U$ of river waters	-0.3	‰	(6) (11)
$[U]_{modern}$	Modern seawater U concentration	1.39×10^{-8}	mol/dm^3	(12), (9)
δ_{modern}	Modern seawater $\delta^{238}U$	-0.4	‰	(9), (11)
Δ_{ox}	Fractionation factor between oxic sink and seawater	0.005	‰	see text and table 4
Δ_{subox}	Fractionation factor between suboxic sink and seawater	0.1	‰	(9)
Δ_{anox}	Fractionation factor between anoxic sink and seawater	0.6	‰	reviewed in (11)
V	Seawater volume	1.37×10^{21}	dm^3	(4)
A	Total seafloor area	3.61×10^{16}	dm^2	(2)
	Modern anoxic seafloor area	0.35	%	(8)
	Modern suboxic seafloor area	6.00	%	(3)
	Modern oxic seafloor area	93.65	%	Balance

References: (1) Andersen and others, 2014; (2) Barnes and Cochran, 1990; (3) Dunk and others, 2002; (4) Hastings and others, 1996; (5) Holmden and others, 2015; (6) Noordmann and others, 2010; (7) Romaniello, 2012 ; (8) Veeh, 1968; (9) Weyer and others, 2008; (10) Morford and Emerson, 1999; (11) Tissot and Dauphas, 2015; (12) Chen and others, 1986.

*Calculated by equation (5) using modern flux, seawater U concentration, and seafloor area associated with each type of sink.

The flux data are chosen from previous studies so that they satisfy modern mass balance as described by equation (4). When fractionation factors were varied in subsequent sensitivity tests, these sink fluxes will change slightly for the same reason. "dm" denotes decimeter.

μmol/L, suboxic as $0 < [O_2] \leq 10$ μmol/L and $[H_2S \leq 10$ μmol/L), and finally oxic as $[O_2] > 10$ μmol/L.

Note that in this modeling exercise several types of sinks are lumped into a single oxic sink, including Fe-Mn crusts, pelagic clays, oceanic crust alteration, and carbonates. Carbonates have been found to be isotopically fractionated from modern seawater by approximately 0.2 permil (Tissot and Dauphas, 2015 and references therein). Fe-Mn crusts are isotopically fractionated from seawater by about -0.24 permil (Brennecka and others, 2011b; Goto and others, 2014). Existing data on pelagic sediments suggest a very small fractionation from seawater (0.04‰, Andersen and others, 2014). Altered oceanic basalts are fractionated from seawater by up to +0.25 permil (Tissot and Dauphas, 2015). Taking the flux data for these individual oxic sinks summarized in Goto and others (2014) (table 4), the overall fractionation factor of the lumped oxic sink from seawater is calculated as the weighted average of these individual sinks, which is 0.005 permil.

Uranium isotope fractionation factors for anoxic and suboxic sinks have been estimated previously (see Tissot and Dauphas, 2015 for a review). The isotope

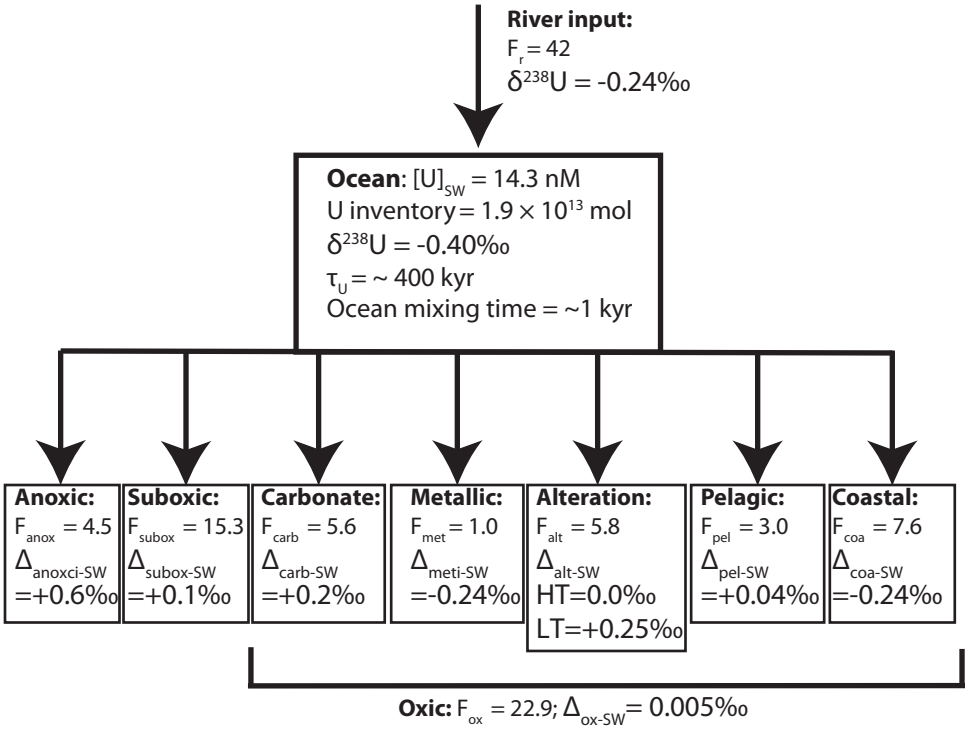

Fig. 5. A simplified schematic representation of the modern U budget. Detailed discussion about the budget can be found in Tissot and Dauphas (2015). Riverine input is assumed to be the only source of U to the ocean: aeolian and groundwater sources are ignored because of their small contributions. Sinks including carbonates, metallic deposits (for example, Fe-Mn crusts), oceanic crust alteration (high temperature, HT, and low temperature, LT), pelagic clay, and coastal retention are treated as one single oxic sink, with the fractionation factors being the weighted average of these individual sinks (see table 4). All flux data have a unit of 10^6 mol/yr.

fractionation factors for anoxic sinks are relatively large and current estimates range from +0.4 permil to +0.85 permil (Weyer and others, 2008; Bopp and others, 2010; Romaniello, ms, 2012; Andersen and others, 2014; Basu and others, 2014; Holmden and others, 2015; Noordmann and others, 2015; Stirling and others, 2015; Stylo and others, 2015). Following previous modeling studies (Montoya-Pino and others, 2010; Brennecka and others, 2011a; Goto and others, 2014; Tissot and Dauphas, 2015), +0.6 permil is chosen as the average fractionation factor for anoxic sinks from seawater for our baseline model. The isotope fractionation factor associated with suboxic sinks is less well constrained, and is expected to vary as a function of sediment oxygen penetration depth (Bender, 1990; Clark and Johnson, 2008; Andersen and others, 2014; Reinhard and others, 2014). The +0.1 permil fractionation factor for suboxic sinks used in this study and previous studies (Montoya-Pino and others, 2010; Brennecka and others, 2011a; Goto and others, 2014; Tissot and Dauphas, 2015) is based on a few measurements of Peru margin sediments by Weyer and others (2008).

Model results are presented in figure 6. We first vary the areal extent of anoxic seafloor area while keeping the areal extent of suboxic seafloor the same as the modern value (solid black curve in figs. 6A and 6B), with oxic seafloor maintaining overall balance. The modeling result shows that with our current understanding of global U mass balance and U isotope fractionation in different marine settings,

TABLE 4

Break down of the oxic sink into individual sinks, together with their isotope fractionation factors from seawater (Δ_i)

	Flux (10^6 mol/yr)	Δ_i (‰)
Pelagic clay	3	+0.04
Carbonates	5.6	+0.2
Metalic seds	1	-0.24
High T oceanic crustal alteration	2.0	0
Low T oceanic crustal alteration	3.8	+0.25
Coastal zone retention	7.6	-0.24
Weighted average		+0.005

The overall U isotope fractionation factor for the lumped oxic sink is calculated as the weighted average of individual ones.

seawater U concentration and $\delta^{238}U$ both decrease as anoxic seafloor area increases. However, with current analytical uncertainty on $\delta^{238}U$ measurement ($\pm 0.07‰$), the anoxic seafloor fraction has varied by no more than ~3 times the modern value (0.21%–0.35% of total seafloor area, Veeh, 1968; Bertine and Turekian, 1973; Tissot and Dauphas, 2015). In reality, however, suboxic seafloor area is likely to covary with anoxic seafloor area. The effect of this scenario is also shown figures 6A and 6B again with the areal extent of oxic seafloor area being balanced accordingly in each model scenario. The results show that suboxic seafloor area variation has a very small effect on our basic conclusion.

The crossover between red and blue lines in figures 6B, 6D, and 6F highlights an important point. For instance, in figure 6B an increase in anoxic seafloor area by a factor of 3 brings the seawater $\delta^{238}U$ from modern value of -0.40 permil down to -0.49 permil, keeping suboxic seafloor unchanged. However, if the increase in anoxic seafloor area is accompanied by a concurrent increase in suboxic seafloor area from a modern value of 6 percent to 20 percent, seawater $\delta^{238}U$ is reduced by a slightly smaller offset. In reality, however, it is also likely that anoxic seafloor area expands at the expense of suboxic seafloor. In this case, the drawdown in seawater $\delta^{238}U$ is slightly enhanced (down to -0.51‰). Although the difference is small under the scenarios examined here, it highlights the necessity to explicitly consider variation of the areal extent of suboxic seafloor when using ancient $\delta^{238}U$ data to interpret anoxic seafloor areal extent variations.

We note that there are substantial uncertainties on current estimates of the U isotope fractionation factors (Δ_i) associated with suboxic and anoxic sinks. However, after incorporating these uncertainties (figs. 6C-6F) into our model exercises, our basic conclusion remains the same – the anoxic seafloor areal extent has varied by less than a factor of 3 from the modern value. This basic conclusion is broadly consistent with conclusions based on the Mo isotope system (Siebert and others, 2003).

Implications of Ocean Deoxygenation

The invariant Cenozoic $\delta^{238}U$ values recorded in Fe-Mn crusts suggest that benthic anoxia has remained remarkably stable on a broad scale. This observation is somewhat surprising given the expectation of low oxygen levels in the warmer climate of the early to middle Cenozoic. A ~10 °C surface temperature change over the last 60 Myr should have caused >65 μmol L^{-1} decreases in dissolved O_2 in the surface ocean

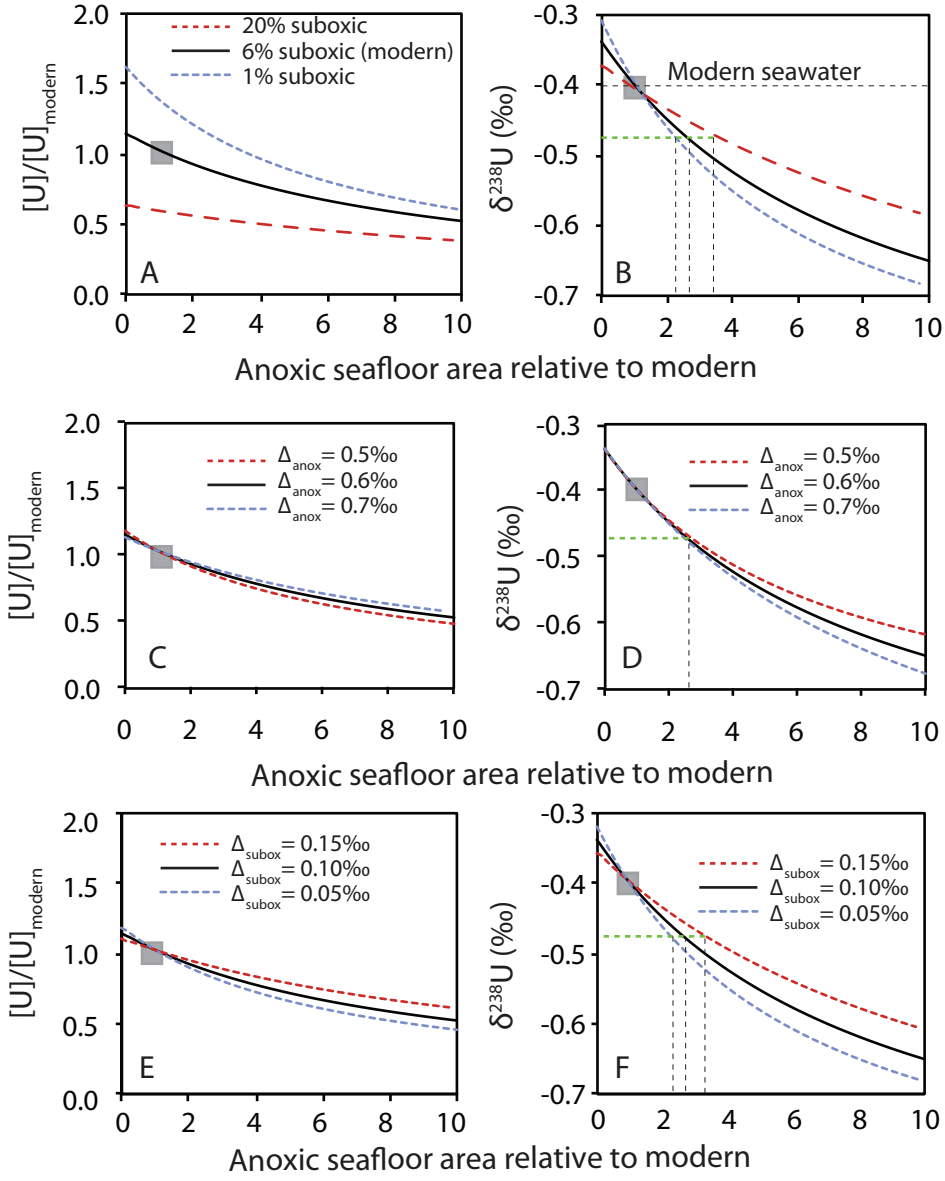

Fig. 6. Results from isotope mass balance model discussed in the text. The shaded boxes denote modern conditions. In B, D, and E, the horizontal dashed line represents the modern seawater minus the analytical uncertainty (0.07‰), with the vertical dashed lines denoting the uncertainties on our reconstructed anoxic seafloor area. With an analytical uncertainty of ±0.07‰ on seawater $\delta^{238}U$ reconstruction, anoxic seafloor area has remained less than ~1% of the total seafloor area (~3 times the modern value). This basic conclusion is not changed after considering potential concurrent variation of suboxic seafloor area, and considering uncertainties on the fractionation factors of anoxic (C and D) and suboxic (E and F) sinks. For C to F, different fractionation factors were input into the same model exercises as in A and B, with the suboxic seafloor area fixed at the modern value (6% of total seafloor area), and oxic seafloor area being balanced. Note that fractionation factors have effects on U concentrations (C and E) because modifying fractionation factors requires rebalancing different sink fluxes to satisfy the modern U isotope mass balance in the ocean as described by equation (4). For interpretation of colors the reader is referred to the web version of this article.

based purely on gas exchange. With all other factors affecting marine oxygen levels being held constant, this should have caused well over an order of magnitude increase in ocean anoxia compared to today, given the spatial distribution of modern low oxygen surface water (Weiss, 1970; Jaccard and Galbraith, 2012). Specifically, approximately 15 percent of the upper 1.5 km of today's ocean, the most biogeochemically active part of the marine realm, is characterized by <65 μmol L^{-1} dissolved oxygen levels (Jaccard and Galbraith, 2012). In addition, approximately 8 percent of the shallow ocean is occupied by OMZs with <20 μmol L^{-1} O_2 (Paulmier and Ruiz-Pino, 2009). Further, the most recent efforts to model atmospheric oxygen levels suggest slightly lower atmospheric pO_2 during the early and middle Cenozoic (for example, Berner, 2006). All these factors discussed above should have driven the shallow oceans toward lower oxygen conditions in the early to middle Cenozoic. In response to decreased surface seawater oxygen levels, and potentially to increased ocean stratification due to warming, the deep ocean should also have experienced decreased oxygen levels.

The stark contrast between our finding and O_2-solubility-based expectation suggests that benthic marine redox, and by inference water column oxygenation on a broad scale, has been somehow stabilized against a backdrop of large changes in tectonic activity, Earth surface temperatures, and ocean circulation. Marine dissolved oxygen concentrations reflect the balance between oxygen supply via gas-water equilibration at the surface and oxygen consumption throughout the water column. Given the expected markedly lower saturation oxygen concentrations on the surface during the early and middle Cenozoic, the redox stability suggested by our U isotope data implies broad decreases in oxygen consumption during the same period.

We suggest that decreased oxygen consumption was probably due to decreased primary productivity. Intense local primary productivity has been suggested to be the prerequisite of ocean anoxia (Pedersen and Calvert, 1990). Anoxic conditions in the modern open ocean are rare because of inhibited N fixation and thus primary productivity. This is due to Fe-P co-limitation (for example, Mills and others, 2004) and intense nutrient-N loss from the marine system due to denitrification and anaerobic ammonium oxidation (Kuypers and others, 2003; Kuypers and others, 2005; Ward and others, 2009). In fact, enhanced denitrification has been suggested to accompany oceanic anoxic events in a greenhouse climate (Jenkyns and others, 2001; Junium and Arthur, 2007). This negative feedback between ocean oxygenation and the nitrogen cycle provides a potential stabilizing mechanism—at least in localized low oxygen zones—that may have prevented the large-scale expansion of anoxic seafloor area (Canfield, 2006; Boyle and others, 2013).

The effect of warming-induced ocean stratification on ocean oxygen levels is not as straightforward. It is generally agreed that warmer climate (for example, the early to middle Cenozoic) tends to cause ocean stratification due to freshening of high-latitude surface water (Sarmiento and others, 1998; Keeling and Garcia, 2002; Zachos and others, 2008). The effects of stratification on ocean oxygen levels are two-fold: On the one hand, more intense stratification will in general reduce oxygen supply to the deep ocean. On the other hand, stratification also reduces nutrient fluxes to the photic zone (Behrenfeld and others, 2006). When there is less organic matter produced, there is less oxygen demand in the water column. Although the net effect of thermal stratification seems to decrease ocean oxygen levels on short time scales (for example, Sarmiento and others, 1998; Keeling and Garcia, 2002), the long time scale effect (a few million years) is still unclear (Zachos and others, 2008).

Although potential stabilizing feedbacks may have prevented large-scale shifts in ocean redox during the Cenozoic, sporadic ocean anoxic events (OAEs) apparently occurred during the Paleozoic and Mesozoic. Moving forward, it will be important to

establish why certain internal stabilization mechanisms work effectively for some time periods but not others. For example, Cretaceous OAEs have been attributed to multiple phenomena acting synergistically, including climate optima, realignment of major ocean current systems, and release of volcanic CO_2 or methane gas hydrate (Jenkyns and others, 2001; Jenkyns, 2010). Certain combinations of forcing may thus conspire to overwhelm the stabilizing influence of, for example, redox-nutrient feedbacks in oxygen-deficient zones of the oceans.

It is important to emphasize that the effects of transient events [for example, the Paleocene-Eocene Thermal Maximum; see Dickson and Cohen (2012) and Dickson and others (2012)] on ocean oxygenation would be unlikely to register at the temporal precision of the records obtained from Fe-Mn crusts. The reason is that these events lasted for only short time periods (for example, the PETM only lasted for ~0.17 Myr, Röhl and others, 2007) which is much shorter than the ~3 Myr diffusional smoothing we observe in Fe-Mn crusts. Shorter transient perturbations in benthic marine redox are important to explore, but will require archives with higher sedimentation rates and proxies with faster response time.

CONCLUDING REMARKS

A new U isotope record from hydrogenous ferromanganese crusts sampled from three major oceans at different ocean depths yields invariant $\delta^{238}U$ values. Combined with a simple isotope mass balance model, we suggest that the spatial extent of anoxic seafloor throughout the Cenozoic has remained with a factor of 3 of the modern value, well below ~1 percent of total seafloor area. This implies a system of long-term feedbacks that has maintained a remarkably stable state of internal ocean oxygen despite large changes in tectonic activity, weathering, nutrient delivery, Earth surface temperature, and ocean circulation. However, this conclusion is only applicable on ~3 Myr time scales due to a diffusional smoothing effect. Sediments with higher accumulation rates and proxy systems with more rapid response times will be required to explore shorter transient perturbations to ocean oxygenation.

ACKNOWLEDGMENTS

This work was supported by the Agouron Institute Geobiology Postdoctoral Fellowship Program, the NASA Exobiology Program, and the Afred P. Slogan Foundation. We thank Associate Editor Freidhelm von Blanckenburg, reviewer Stephen Romaniello, and two anonymous reviewers for providing comments that helped improve the quality of the original manuscript.

APPENDIX

Methods

A ^{233}U-^{236}U double spike method was used to correct for instrumental mass bias and potential isotopic fractionation during sample preparation (Weyer and others, 2008; Shiel and others, 2013). The double spike method also allowed isotope dilution calculations for U concentrations, based on measured $^{238}U/^{236}U$ and the amount of double spike added. Sample aliquots with 300 ng U were spiked with appropriate amount of double spike to yield a $^{238}U/^{236}U$ ratio of ~30. The sample-spike mixtures were then slowly evaporated to dryness and redissolved in 3 N HNO_3.

Samples were purified with the UTEVA ion exchange resin (based on ref. Weyer and others, 2008). Briefly, U samples in 3 N HNO_3 were loaded onto 0.2 mL UTEVA resin columns (inner diameter of 0.33 mm) pre-cleaned with 4 mL 0.05 N HCl and preconditioned with 1 mL 3 N HNO_3. Matrix elements were eluted with 2 ml 3 N HNO_3. Thorium was eluted with 2 mL 3 N HCl (Rožmarić and others, 2009). U was then released from the resin with 2.5 mL 0.05 N HCl. Collected U samples were evaporated to dryness and treated with a few drops of concentrated distilled HNO_3 to destroy potential residual organics leached from the resin.

Purified U samples were dissolved in 2 mL 0.3 N HNO_3 and introduced into the MC-ICP-MS with a DSN 100 desolvating system (Nu Instrument, UK) housed at Department of Geology, University of Illinois at Urbana-Champaign. Detailed information on instrument parameters and analysis routines can be found in Shiel and others (2013) and Wang and others (2015). Briefly, isotopes ^{232}Th, ^{233}U, ^{234}U, ^{235}U, ^{236}U and ^{238}U were measured simultaneously on Faraday collectors connected to 10^{11} Ω amplifiers, except that ^{238}U was measured with a Faraday connected to 10^{10} Ω amplifier yielding 30–40 volt ^{238}U signal.

The CRM 112a (New Brunswick Laboratory, U.S. Department of Energy) standard was analyzed every 3 samples to monitor drift in instrumental mass bias. The $\delta^{238}U$ and ($^{234}U/^{238}U$) values of samples were normalized to the average values of the bracketing CRM 112a, assuming $\delta^{238}U_{CRM\ 112a} = 0‰$ and $(^{234}U/^{238}U)_{CRM\ 112a} = 0.9619$. ($^{234}U/^{238}U$) values are calculated using decay constants for ^{238}U and ^{234}U of 1.55×10^{-10} and 2.83×10^{-6}, respectively (Cheng and others, 2013; Villa and others, 2016). Secondary standards IRMM REIMP 18a (JRC, Brussels, Belgium) and CRM 129 (New Brunswick Laboratory, U.S. Department of Energy) measured in each session before samples yielded $\delta^{238}U$ values of -0.17±0.09‰ (2SD, n = 5) and −1.77±0.07 (2 SD, n = 5), respectively, consistent with other studies (Weyer and others, 2008; Shiel and others, 2013). External uncertainties for $\delta^{238}U$, U concentration, and ($^{234}U/^{238}U$) measurements were ±0.07‰, ±0.1 μg g^{-1}, and 3.7‰ at 95% confidence level, respectively, calculated as the root mean square difference of six duplicate sample preparations and analyses (Hyslop and White, 2009). Procedural blank was ~ 10–40 pg, which was negligible (<0.01%) compared to 300 ng sample U.

References

Andersen, M. B., Romaniello, S., Vance, D., Little, S. H., Herdman, R., and Lyons, T. W., 2014, A modern framework for the interpretation of $^{238}U/^{235}U$ in studies of ancient ocean redox: Earth and Planetary Science Letters, v. 400, p. 184–194, http://dx.doi.org/10.1016/j.epsl.2014.05.051

Andersen, M. B., Vance, D., Morford, J. L., Bura-Nakić, E., Breitenbach, S. F. M., and Och, L., 2016, Closing in on the marine $^{238}/^{235}U$ budget: Chemical Geology, v. 420, p. 11–22, http://dx.doi.org/10.1016/j.chemgeo.2015.10.041

Anderson, R. F., Fleisher, M. Q., and LeHuray, A. P., 1989, Concentration, oxidation state, and particulate flux of uranium in the Black Sea: Geochimica et Cosmochimica Acta, v. 53, n. 9, p. 2215–2224, http://dx.doi.org/10.1016/0016-7037(89)90345-1

Barnes, C. E., and Cochran, J. K., 1990, Uranium removal in oceanic sediments and the oceanic U balance: Earth and Planetary Science Letters, v. 97, n. 1–2, p. 94–101, http://dx.doi.org/10.1016/0012-821X(90)90101-3

Basu, A., Sanford, R. A., Johnson, T. M., Lundstrom, C. C., and Löfler, F. E., 2014, Uranium Isotopic Fractionation Factors during U(VI) Reduction by Bacterial Isolates: Geochimica et Cosmochimica Acta, v. 136, p. 100–113, http://dx.doi.org/10.1016/j.gca.2014.02.041

Behrenfeld, M. J., O'Malley, R. T., Siegel, D. A., McClain, C. R., Sarmiento, J. L., Feldman, G. C., Milligan, A. J., Falkowski, P. G., Letelier, R. M., and Boss, E. S., 2006, Climate-driven trends in contemporary ocean productivity: Nature, v. 444, p. 752–755, http://dx.doi.org/10.1038/nature05317

Bender, M. L., 1990, The $\delta^{18}O$ of dissolved O_2 in seawater: A unique tracer of circulation and respiration in the deep sea: Journal of Geophysical Research- Oceans, v. 95, n. C2, p. 22243–22252, http://dx.doi.org/10.1029/JC095iC12p22243

Berner, R. A., 1981, A new geochemical classification of sedimentary environments: Journal of Sedimentary Research, v. 51, n. 2, p. 359–365, http://dx.doi.org/0.1306/212F7C7F-2B24-11D7-8648000102C1865D

——— 2006, GEOCARBSULF: A combined model for Phanerozoic atmospheric O_2 and CO_2: Geochimica et Cosmochimica Acta, v. 70, n. 23, p. 5653–5664, http://dx.doi.org/10.1016/j.gca.2005.11.032

Bertine, K. K., and Turekian, K. K., 1973, Molybdenum in marine deposits: Geochimica et Cosmochimica Acta, v. 37, n. 6, p. 1415–1434, http://dx.doi.org/10.1016/0016-7037(73)90080-X

Bopp, C. J., IV, Lundstrom, C. C., Johnson, T. M., Sanford, R. A., Long, P. E., and Williams, K. H., 2010, Uranium $^{238}U/^{235}U$ isotope ratios as indicators of reduction: Results from an *in situ* biostimulation experiment at Rifle, Colorado, USA: Environmental Science & Technology, v. 44, p. 5927–5933, http://dx.doi.org/10.1021/es100643v

Bourdon, B., Turner, S., Henderson, G. M., and Lundstrom, C. C., 2003, Introduction to U-series geochemistry: Reviews in Mineralogy and Geochemistry, v. 52, n. 1, p. 1–21, http://dx.doi.org/10.2113/0520001

Boyle, R. A., Clark J. R., Poulton, S. W., Shields-Zhou, G., Canfield, D. E., and Lenton T. M., 2013, Nitrogen cycle feedbacks as a control on euxinia in the mid-Proterozoic ocean: Nature Communications, v. 4, p. 1533, http://dx.doi.org/10.1038/ncomms2511

Brennecka, G. A., Herrmann, A. D., Algeo, T. J., and Anbar, A. D., 2011a, Rapid expansion of oceanic anoxia immediately before the end-Permian mass extinction: Proceedings of the National Academy of Sciences of the United States of America, v. 108, p. 17631–17634, http://dx.doi.org/10.1073/pnas.1106039108

Brennecka, G. A., Wasylenki, L. E., Bargar, J. R., Weyer, S., and Anbar, A. D., 2011b, Uranium Isotope Fractionation during Adsorption to Mn-Oxyhydroxides: Environmental Science & Technology, v. 45, n. 4, p. 1370–1375, http://dx.doi.org/10.1021/es103061v

Broecker, W. S., and Peng T-H., 1982, Tracers in the Sea: Acta Chemica Scandinavica, Series A: Physical and Inorganic Chemistry: Palisades, New York, USA, Lamont-Doherty Geological Observatory, 690 p.

Burton, K. W., 2006, Global weathering variations inferred from marine radiogenic isotope records: Journal of Geochemical Exploration, v. 88, n. 1–3, p. 262–265, http://dx.doi.org/10.1016/j.gexplo.2005.08.052
Canfield, D. E., 2006, Models of oxic respiration, denitrification and sulfate reduction in zones of coastal upwelling: Geochimica et Cosmochimica Acta, v. 70, n. 23, p. 5753–5765, http://dx.doi.org/10.1016/j.gca.2006.07.023
Chen, J. H., and Wasserburg, G. J., 1981, Precise isotopic analysis of uranium in picomole and subpicomole quantities: Analytical Chemistry, v. 53, n. 13, p. 2060–2067, http://dx.doi.org/10.1021/ac00236a027
Chen, J. H., Edwards, R. L., and Wasserburg, G. J., 1986, ^{238}U, ^{234}U and ^{232}Th in seawater: Earth and Planetary Science Letters, v. 80, n. 3–4, p. 241–251., http://dx.doi.org/10.1016/0012-821X(86)90108-1
Cheng, H., Edwards, R. L., Hoff, J., Gallup, C. D., Richards, D. A., and Asmerom Y., 2000, The half-lives of uranium-234 and thorium-230: Chemical Geology, v. 169, n. 1–2, p. 17–33, http://dx.doi.org/10.1016/S0009-2541(99)00157-6
Cheng, H., Edwards, R. L., Shen, C.-C., Polyak, V. J., Asmerom, Y., Woodhead, J., Hellstrom, J., Wang, Y., Kong, X., Spötl, C., Wang, X., and Alexander, E. A., Jr., 2013, Improvements in ^{230} Th dating, ^{230}Th and ^{234}U half-life values, and U–Th isotopic measurements by multi-collector inductively coupled plasma mass spectrometry: Earth and Planetary Science Letters, v. 371–372, p. 82–91, http://dx.doi.org/10.1016/j.epsl.2013.04.006
Clark, S. K., and Johnson, T. M., 2008, Effective isotopic fractionation factors for solute removal by reactive sediments: A laboratory microcosm and slurry study: Environmental Science & Technology, v. 42, n. 21, p. 7850–7855, http://dx.doi.org/10.1021/es801814v
DePaolo, D. J., Maher, K., Christensen, J. N., and McManus, J., 2006, Sediment transport time measured with U-series isotopes: Results from ODP North Atlantic drift site 984: Earth and Planetary Science Letters, v. 248, n. 1–2, p. 394–410, http://dx.doi.org/10.1016/j.epsl.2006.06.004
Dickson, A. J., and Cohen, A. S., 2012, A molybdenum isotope record of Eocene Thermal Maximum 2: Implications for global ocean redox during the early Eocene: Paleoceanography, v. 27, n. 3, p. PA3230, http://dx.doi.org/10.1029/2012PA002346
Dickson, A. J., Cohen, A. S., and Coe, A. L., 2012, Seawater oxygenation during the Paleocene-Eocene thermal maximum: Geology, v. 40, n. 7, p. 639–642, http://dx.doi.org/10.1130/G32977.1
Dunk, R., Mills, R., and Jenkins, W., 2002, A reevaluation of the oceanic uranium budget for the Holocene: Chemical Geology, v. 190, n. 1–4, p. 45–67, http://dx.doi.org/10.1016/S0009-2541(02)00110-9
Frank, M., O'Nions, R. K., Hein, J. R., and Banakar, V. K., 1999, 60 Myr records of major elements and Pb-Nd isotopes from hydrogenous ferromanganese crusts: Reconstruction of seawater paleochemistry: Geochimica et Cosmochimica Acta, v. 63, n. 11–12, p. 1689–1708, http://dx.doi.org/10.1016/S0016-7037(99)00079-4
Goto, K. T., Anbar, A. D., Gordon, G. W., Romaniello, S. J., Shimoda, G., Takaya, Y., Tokumaru, A., Nozaki, T., Suzuki, K., Machida, S., Hanyu, T., and Usui, A., 2014, Uranium isotope systematics of ferromanganese crusts in the Pacific Ocean: Implications for the marine $^{238}U/^{235}U$ isotope system: Geochimica et Cosmochimica Acta, v. 146, p. 43–58., http://dx.doi.org/10.1016/j.gca.2014.10.003
Hansen, J., Sato, M., Kharecha, P., Beerling, D., Berner, R., Masson-Delmotte, V., Pagani, M., Raymo, M., Royer, D. L., and Zachos, J. C., 2008, Target atmospheric CO2: Where should humanity aim?: The Open Atmospheric Science Journal, v. 9, n. 2, p. 217–231, http://dx.doi.org/10.2174/1874282300802010217
Hastings, D. W., Emerson, S. R., and Mix, A. C., 1996, Vanadium in foraminiferal calcite as a tracer for changes in the areal extent of reducing sediments: Paleoceanography, v. 11, n. 6, p. 665–678, http://dx.doi.org/10.1029/96PA01985
Hein, J. R., and Koschinsky, A., 2014, Deep-Ocean Ferromanganese Crusts and Nodules, *in* Scott, S. D., editor, Geochemistry of Mineral Deposits: Treatise of Geochemistry, 2nd edition, v. 13, p. 273–291, http://dx.doi.org/10.1016/B978-0-08-095975-7.01111-6
Hein, J. R., Yeh, H. W., Gunn, S. H., Sliter, W. V., Benninger, L. M., and Wang, C. H., 1993, Two major Cenozoic episodes of phosphogenesis recorded in equatorial Pacific seamount deposits: Paleoceanography, v. 8, n. 2, p. 293–311, http://dx.doi.org/10.1029/93PA00320
Helly, J. J., and Levin, L. A., 2004, Global distribution of naturally occurring marine hypoxia on continental margins: Deep Sea Research Part I: Oceanographic Research Papers, v. 51, n. 9, p. 1159–1168, http://dx.doi.org/10.1016/j.dsr.2004.03.009
Henderson, G. M., 2002, Seawater ($^{234}U/^{238}U$) during the last 800 thousand years: Earth and Planetary Science Letters, v. 199, n. 1–2, p. 97–110, http://dx.doi.org/10.1016/S0012-821X(02)00556-3
Henderson, G. M., and Burton, K. W., 1999, Using ($^{234}U/^{238}U$) to assess diffusion rates of isotope tracers in ferromanganese crusts: Earth and Planetary Science Letters, v. 170, n. 3, p. 169–179, http://dx.doi.org/10.1016/S0012-821X(99)00104-1
Holmden, C., Amini, M., and Francois, R., 2015, Uranium isotope fractionation in Saanich Inlet: A modern analog study of a paleoredox tracer: Geochimica et Cosmochimica Acta, v. 153, p. 202–215, http://dx.doi.org/10.1016/j.gca.2014.11.012
Horwitz, E. P., Chiarizia, R., Dietz, M. L., Diamond, H., and Nelson, D. M., 1993, Separation and preconcentration of actinides from acidic media by extraction chromatography: Analytica Chimica Acta, v. 281, n. 2, p. 361–372, http://dx.doi.org/10.1016/0003-2670(93)85194-O
Hyslop, N. P., and White, W. H., 2009, Estimating precision using duplicate measurements: Journal of the Air & Waste Management Association, v. 59, n. 9, p. 1032–1039, http://dx.doi.org/10.3155/1047-3289.59.9.1032
Jaccard, S. L., and Galbraith, E. D., 2012, Large climate-driven changes of oceanic oxygen concentrations during the last deglaciation: Nature Geoscience, v. 5, p. 151–156, http://dx.doi.org/10.1038/ngeo1352
Jaffey, A. H., Flynn, K. F., Glendenin, L. E., Bentley, W. C., and Essling, A. M., 1971, Precision measurement of half-lives and specific activities of ^{235}U and ^{238}U: Physical Review C, v. 4, n. 5, p. 1889, http://dx.doi.org/10.1103/PhysRevC.4.1889

Jenkyns, H. C., 2010, Geochemistry of oceanic anoxic events: Geochemistry, Geophysics, Geosystems, v. 11, n. 3, p. Q03004, http://dx.doi.org/10.1029/2009GC002788
Jenkyns H. C., Gröcke D. R., and Hesselbo, S. P., 2001, Nitrogen isotope evidence for water mass denitrification during the early Toarcian (Jurassic) oceanic anoxic event: Paleoceanography, v. 16, n. 6, p. 593–603, http://dx.doi.org/10.1029/2000PA000558
Junium, C. K., and Arthur, M. A., 2007, Nitrogen cycling during the Cretaceous, Cenomanian-Turonian oceanic anoxic event II: Geochemistry, Geophysics, Geosystems, v. 8, p. Q03002, http://dx.doi.org/10.1029/2006GC001328
Keeling, R. F., and Garcia, H. E., 2002, The change in oceanic O_2 inventory associated with recent global warming: Proceedings of the National Academy of Sciences of the United States of America, v. 99, n. 12, p. 7848–7853, http://dx.doi.org/10.1073/pnas.122154899
Keeling, R. F., Körtzinger, A., and Gruber, N., 2010, Ocean deoxygenation in a warming world: Annual Review of Marine Science, v. 2, p. 199–229, http://dx.doi.org/10.1146/annurev.marine.010908.163855
Klemm, V., Levasseur, S., Frank, M., Hein, J. R., and Halliday, A. N., 2005, Osmium isotope stratigraphy of a marine ferromanganese crust: Earth and Planetary Science Letters, v. 238, n. 1–2, p. 42–48, http://dx.doi.org/10.1016/j.epsl.2005.07.016
Klemm, V., Frank, M., Levasseur, S., Halliday, A. N., and Hein, J. R., 2008, Seawater osmium isotope evidence for a middle Miocene flood basalt event in ferromanganese crust records: Earth and Planetary Science Letters, v. 273, n. 1–2, p. 175–183, http://dx.doi.org/10.1016/j.epsl.2008.06.028
Koschinsky, A., and Halbach, P., 1995, Sequential leaching of marine ferromanganese precipitates: Genetic implications: Geochimica et Cosmochimica Acta, v. 59, n. 24, p. 5113–5132, http://dx.doi.org/10.1016/0016-7037(95)00358-4
Koschinsky, A., and Hein, J. R., 2003, Uptake of elements from seawater by ferromanganese crusts: solid-phase associations and seawater speciation: Marine Geology, v. 198, n. 3–4, p. 331–351, http://dx.doi.org/10.1016/S0025-3227(03)00122-1
Ku, T.-L., Knauss, K. G., and Mathieu, G. G., 1977, Uranium in open ocean: concentration and isotopic composition: Deep Sea Research, v. 24, n. 11, p. 1005–1017, http://dx.doi.org/10.1016/0146-6291(77)90571-9
Kuypers, M. M. M., Sliekers, A. O., Lavik, G., Schmid, M., Jørgensen, B. B., Kuenen, J. G., Damsté, J. S. S., Strous, M., and Jetten, M. S. M., 2003, Anaerobic ammonium oxidation by anammox bacteria in the Black Sea: Nature, v. 422, p. 608–611.
Kuypers, M. M. M., Lavik, G., Woebken, D., Schmid, M., Fuchs, B. M., Amann, R., Jørgensen, B. B., and Jetten, M. S., 2005, Massive nitrogen loss from the Benguela upwelling system through anaerobic ammonium oxidation: Proceedings of the National Academy of Sciences of the United States of America, v. 102, n. 18, p. 6478–6483, http://dx.doi.org/10.1073/pnas.0502088102
Langmuir, D., 1978, Uranium solution-mineral equilibria at low temperatures with applications to sedimentary ore deposits: Geochimica et Cosmochimica Acta, v. 42, n. 6, Part A, p. 547–569, http://dx.doi.org/10.1016/0016-7037(78)90001-7
Ling, H. F., Burton, K. W., O'Nions, R. K., Kamber, B. S., von Blanckenburg, F., Gibb, A. J., and Hein, J. R., 1997, Evolution of Nd and Pb isotopes in Central Pacific seawater from ferromanganese crusts: Earth and Planetary Science Letters, v. 146, n. 1–2, p. 1–12, http://dx.doi.org/10.1016/S0012-821X(96)00224-5
Mills, M. M., Ridame, C., Davey, M., La Roche, J., and Geider, R. J., 2004, Iron and phosphorus co-limit nitrogen fixation in the eastern tropical North Atlantic: Nature, v. 429, p. 292–294, http://dx.doi.org/10.1038/nature02550
Montoya-Pino, C., Weyer, S., Anbar, A. D., Pross, J., Oschmann, W., van de Schootbrugge, B., and Arz, H. W., 2010, Global enhancement of ocean anoxia during Oceanic Anoxic Event 2: A quantitative approach using U isotopes: Geology, v. 38, n. 4, p. 315–318, http://dx.doi.org/10.1130/G30652.1
Morford, J. L., and Emerson, S., 1999, The geochemistry of redox sensitive trace metals in sediments: Geochimica et Cosmochimica Acta, v. 63, n. 11–12, p. 1735–1750, http://dx.doi.org/10.1016/S0016-7037(99)00126-X
Murray, J. W., Stewart, K., Kassakian, S., Krynytzky, M., and DiJulio, D., 2007, Oxic, suboxic, and anoxic conditions in the Black Sea, *in* Yanko-Hombach, V., Gilbert, A. S., Panin, N., and Dolukhanov, P. M., editors, The Black Sea Flood Question: Changes in Coastline, Climate, and Human Settlement, p. 1–21.
Nielsen, S. G., Mar-Gerrison, S., Gannoun, A., LaRowe, D., Klemm, V., Halliday, A. N., Burton, K. W., and Hein, J. R., 2009, Thallium isotope evidence for a permanent increase in marine organic carbon export in the early Eocene: Earth and Planetary Science Letters, v. 278, n. 3–4, p. 297–307, http://dx.doi.org/10.1016/j.epsl.2008.12.010
Nielsen, S. G., Gannoun, A., Marnham, C., Burton, K. W., Halliday, A. N., and Hein, J. R., 2011, New age for ferromanganese crust 109D–C and implications for isotopic records of lead, neodymium, hafnium, and thallium in the Pliocene Indian Ocean: Paleoceanography, v. 26, p. PA2213, http://dx.doi.org/10.1029/2010PA002003
Noordmann, J., Weyer, S., Sharma, M., Georg, R., Rausch, S., and Bach, W., 2010, Fractionation of 238U/235U in rivers and hydrothermal systems: Constraints for the oceanic U isotope cycle: San Francisco, California, American Geophysical Union Fall Meeting, abstract # V31B-2330.
Noordmann, J., Weyer, S., Georg, R. B., Jöns, S., and Sharma, M., 2015, $^{238}U/^{235}U$ isotope ratios of crustal material, rivers and products of hydrothermal alteration: New insights on the oceanic U isotope mass balance: Isotopes in Environmental and Health Studies, p. 1–23, http://dx.doi.org/10.1080/10256016.2015.1047449.
O'Nions, R. K., Frank, M., von Blanckenburg, F., and Ling, H.-F., 1998, Secular variation of Nd and Pb isotopes in ferromanganese crusts from the Atlantic, Indian and Pacific Oceans: Earth and Planetary Science Letters, v. 155, n. 1–2, p. 15–28, http://dx.doi.org/10.1016/S0012-821X(97)00207-0
Partin, C. A., Bekker, A., Planavsky, N. J., Scott, C. T., Gill, B. C., Li, C., Podkovyrov, V., Maslov, A.,

Konhauser, K. D., Lalonde, S. V., Love, G. D., Poulton, S. W., and Lyons, T. W., 2013, Large-scale fluctuations in Precambrian atmospheric and oceanic oxygen levels from the record of U in shales: Earth and Planetary Science Letters, v. 369–370, p. 284–293, http://dx.doi.org/10.1016/j.epsl.2013.03.031

Paulmier, A., and Ruiz-Pino, D., 2009, Oxygen minimum zones (OMZs) in the modern ocean: Progress in Oceanography, v. 80, n. 3–4, p. 113–128, http://dx.doi.org/10.1016/j.pocean.2008.08.001

Pedersen, T. F., and Calvert, S. E., 1990, Anoxia vs. Productivity: What Controls the Formation of Organic-Carbon-Rich Sediments and Sedimentary Rocks?: AAPG Bulletin, v. 74, p. 454–466.

Puteanus, D., and Halbach, P., 1988, Correlation of Co concentration and growth rate—a method for age determination of ferromanganese crusts: Chemical Geology, v. 69, n. 1–2, p. 73–85, http://dx.doi.org/10.1016/0009-2541(88)90159-3

Rademacher, L. K., Lundstrom, C. C., Johnson, T. M., Sanford, R. A., Zhao, J., and Zhang, Z., 2006, Experimentally determined uranium isotope fractionation during reduction of hexavalent U by bacteria and zero valent iron: Environmental Science & Technology, v. 40, n. 22, p. 6943–6948, http://dx.doi.org/10.1021/es0604360

Rehkämper, M., Frank, M., Hein, J. R., Porcelli, D., Halliday, A., Ingri, J., and Liebetrau, V., 2002, Thallium isotope variations in seawater and hydrogenetic, diagenetic, and hydrothermal ferromanganese deposits: Earth and Planetary Science Letters, v. 197, n. 12, p. 65–81, http://dx.doi.org/10.1016/S0012-821X(02)00462-4

Rehkämper, M., Frank, M., Hein, J. R., and Halliday, A., 2004, Cenozoic marine geochemistry of thallium deduced from isotopic studies of ferromanganese crusts and pelagic sediments: Earth and Planetary Science Letters, v. 219, n. 1–2, p. 77–91, http://dx.doi.org/10.1016/S0012-821X(03)00703-9

Reinhard, C. T., Planavsky, N. J., Robbins, L. J., Partin, C. A., Gill, B. C., Lalonde, S. V., Bekker, A., Konhauser, K. O., and Lyons, T. W., 2013, Proterozoic ocean redox and biogeochemical stasis: Proceedings of the National Academy of Sciences of the United States of America, v. 110, n. 14, p. 5357–5362, http://dx.doi.org/10.1073/pnas.1208622110

Reinhard, C. T., Planavsky, N. J., Wang, X., Fischer, W. W., Johnson, T. M., and Lyons, T. W., 2014, The isotopic composition of authigenic chromium in anoxic marine sediments: A case study from the Cariaco Basin: Earth and Planetary Science Letters, v. 407, p. 9–18, http://dx.doi.org/10.1016/j.epsl.2014.09.024

Röhl, U., Westerhold, T., Bralower, T. J., and Zachos, J. C., 2007, On the duration of the Paleocene-Eocene thermal maximum (PETM): Geochemistry, Geophysics, Geosystems, v. 8, n. 12, p. Q12002, http://dx.doi.org 10.1029/2007GC001784

Romaniello, S., ms, 2012, Incorporation and Preservation of Molybdenum and Uranium Isotope Variations in Modern Marine Sediments: Phoenix, Arizona, Arizona State University, Ph. D. thesis, 143 p.

Rožmarić, M., Ivšić, A. G., and Grahek, Ž., 2009, Determination of uranium and thorium in complex samples using chromatographic separation, ICP-MS and spectrophotometric detection: Talanta, v. 80, n. 1, p. 352–362, http://dx.doi.org/10.1016/j.talanta.2009.06.078

Sarmiento, J. L., Hughes, T. M., Stouffer, R. J., and Manabe, S., 1998, Simulated response of the ocean carbon cycle to anthropogenic climate warming: Nature, v. 393, p. 245–249, http://dx.doi.org/10.1038/30455

Schauble, E. A., 2007, Role of nuclear volume in driving equilibrium stable isotope fractionation of mercury, thallium, and other very heavy elements: Geochimica et Cosmochimica Acta, v. 71, n. 9, p. 2170–2189, http://dx.doi.org/10.1016/j.gca.2007.02.004

Shaffer, G., Olsen, S. M., and Pedersen, J. O. P., 2009, Long-term ocean oxygen depletion in response to carbon dioxide emissions from fossil fuels: Nature Geoscience, v. 2, p. 105–109, http://dx.doi.org/10.1038/ngeo420

Shiel, A. E., Laubach, P. G., Johnson, T. M., Lundstrom, C. C., Long, P. E., and Williams, K. H., 2013, No measurable changes in $^{238}U/^{235}U$ due to desorption-adsorption of U(VI) from groundwater at the Rifle, Colorado, Integrated Field Research Challenge Site: Environmental Science & Technology, v. 47, n. 6, p. 2535–2541, http://dx.doi.org/10.1021/es303913y

Siebert, C., Nägler, T. F., von Blanckenburg, F., and Kramers, J. D., 2003, Molybdenum isotope records as a potential new proxy for paleoceanography: Earth and Planetary Science Letters, v. 211, n. 1–2, p. 159–171, http://dx.doi.org/10.1016/S0012-821X(03)00189-4

Stirling, C. H., Halliday, A. N., and Porcelli, D., 2005, In search of live ^{247}Cm in the early solar system: Geochimica et Cosmochimica Acta, v. 69, n. 4, p. 1059–1071, http://dx.doi.org/10.1016/j.gca.2004.06.034

Stirling, C. H., Andersen, M. B., Warthmann, R., and Halliday, A. N., 2015, Isotope fractionation of ^{238}U and ^{235}U during biologically-mediated uranium reduction: Geochimica et Cosmochimica Acta, v. 163, p. 200–218, http://dx.doi.org/10.1016/j.gca.2015.03.017

Stramma, L., Schmidtko, S., Levin, L. A., and Johnson, G. C., 2010, Ocean oxygen minima expansions and their biological impacts: Deep Sea Research Part I: Oceanographic Research Papers, v. 57, n. 4, p. 587–595, http://dx.doi.org/10.1016/j.dsr.2010.01.005

Stylo, M., Neubert, N., Wang, Y., Monga, N., Romaniello, S. J., Weyer, S., and Bernier-Latmani, R., 2015, Uranium isotopes fingerprint biotic reduction: Proceedings of the National Academy of Sciences of the United States of America, v. 112, n. 8, p. 5619–5624, http://dx.doi.org/10.1073/pnas.1421841112

Tissot, F. L., and Dauphas, N., 2015, Uranium isotopic compositions of the crust and ocean: Age corrections, U budget and global extent of modern anoxia: Geochimica et Cosmochimica Acta, v. 167, p. 113–143, http://dx.doi.org/10.1016/j.gca.2015.06.034

Veeh, H. H., 1968, Deposition of uranium from the ocean: Earth and Planetary Science Letters, v. 3, p. 145–150, http://dx.doi.org/10.1016/0012-821X(67)90026-X

Villa, I. M., Bonardi, M. L., De Bièvre, P., Holden, N., and Renne, P., 2016, IUPAC-IUGS status report on the

half-lives of ^{238}U, ^{235}U and ^{234}U: Geochimica et Cosmochimica Acta, v. 172, p. 387–392, http://dx.doi.org/10.1016/j.gca.2015.10.011

Wang, X. L., Johnson, T. M., and Lundstrom, C. C., 2015, Isotope fractionation during oxidation of tetravalent uranium by dissolved oxygen: Geochimica et Cosmochimica Acta, v. 150, p. 160–170, http://dx.doi.org/10.1016/j.gca.2014.12.007

Ward, B. B., Devol, A. H., Rich, J. J., Chang, B. X., Bulow, S. E., Naik, H., Pratihary, A., and Jayakumar, A., 2009, Denitrification as the dominant nitrogen loss process in the Arabian Sea: Nature, v. 461, p. 78–81, http://dx.doi.org/10.1038/nature08276

Weiss, R. F., 1970, The solubility of nitrogen, oxygen and argon in water and seawater: Deep Sea Research and Oceanographic Abstracts, v. 17, n. 4, p. 721–735, http://dx.doi.org/10.1016/0011-7471(70)90037-9

Weyer, S., Anbar, A., Gerdes, A., Gordon, G., Algeo, T., and Boyle, E., 2008, Natural fractionation of $^{238}U/^{235}U$: Geochimica et Cosmochimica Acta, v. 72, n. 2, p. 345–359, http://dx.doi.org/10.1016/j.gca.2007.11.012

Zachos, J. C., Dickens, G. R., and Zeebe, R. E., 2008, An early Cenozoic perspective on greenhouse warming and carbon-cycle dynamics: Nature, v. 451, p. 279–283, http://dx.doi.org/10.1038/nature06588